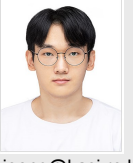


# Double Synchrotron Self-Absorption Spectrum of the Blazar 3C 454.3 and Its Magnetic Field Strength

Hyeon-Woo Jeong and Sang-Sung Lee

Astronomy and Space Science, University of Science and Technology, Daejeon, 34113, Republic of Korea  
Korea Astronomy and Space Science Institute, Daejeon 34055, Korea



hwjeong@kasi.re.kr

## Abstract

The blazar 3C 454.3 is known for its strong outburst across the whole electromagnetic spectrum. Multi-wavelength radio observations enable us to study the spectral variability of relativistic radio jets in the source. In our work, we use multi-wavelength radio observations from 3 GHz to 340 GHz. From the spectral analysis using the multi-wavelength data we found two synchrotron self-absorption(SSA) features in the spectra for the compact variable emission regions in the source. One peak of the SSA spectral features is found at a frequency range of 3-37 GHz (LSS), and the other at 56-124 GHz (HSS). By using the derived SSA turnover frequency and peak flux density, we estimated B-field strength ( $B_{SSA}$ ) for the SSA regions in the relativistic jets. The estimated B-field strengths of the HSS and LSS features are  $>0.2\text{mG}$  and  $>7\text{mG}$ , respectively. The LSS B-field strength is stronger than the estimated B-field strength ( $B_{EQ} = 2-4\text{mG}$ ) under the equipartition condition before the 2014 June  $\gamma$ -ray flare. We found the LSS region is close to the quasi-stationary (C) component  $\sim 0.6$  mas away from the VLBI core at 43GHz. And we found the component C is considered as recollimation shock based on the analysis of jet size and polarization.

## 1. The Blazar 3C 454.3

- One of the most extreme cases among blazars
- The jet component K14 was ejected from 43GHz radio core during the 2014 June  $\gamma$ -ray flaring event (Liodakis et al. 2020)
- The quasi-stationary (C) component  $\sim 0.6$  mas away from 43 GHz radio core

## 2. Typical SSA spectrum

- Synchrotron self-absorption(SSA) is an absorption of synchrotron photons by the electrons in relativistic jets itself as shown in Fig 1.

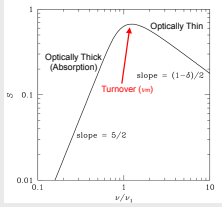


Fig 1. Typical SSA spectrum. If observing frequency is lower than  $\nu_m$ , emission region become optically thick.

## 3. Multi-wavelength Observations

Multi-wavelength single-dish/array and VLBI observations of 3-340 GHz.

Instrument	Obs. Frequency (GHz)	Reference
Effelsberg	2.64, 4.85, 8.35, 10.45, 14.6, 23.05, 32, 43	Fuhrmann et al. 2016
OVRO	15	The OVRO team
KVN	22, 43	The KVN single-dish cross-scan
CARMA	94.75	The MARMOT team
SMA	228.3, 343.04	Public Archive
ALMA	91.5, 103.5, 233, 337, 343.5	Public Archive
EVN	5	Public Archive
VLBA	15, 22, 43	Public Archive 15GHz: MOJAVE (Lister et al. 2018) 43GHz: VLBA-BU-BLAZAR (Jorstad et al. 2017)

Table 1. Instrumentation, observing frequency and reference

## 4. Two SSA Features

Clean 1 Map, 1 Instrument: VLBA 3C454.3, 43.135 GHz, 2013-07-28

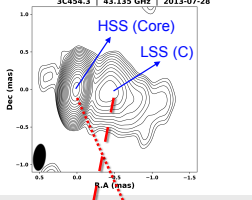


Fig 2. 43 GHz Stokes I map of 3C 454.3 in 2013 July. Observation and data reduction were conducted by VLBA-BU-BLAZAR team. (Jorstad et al. 2017)

LSS : Lower turnover frequency SSA Spectrum  
HSS : Higher turnover frequency SSA Spectrum

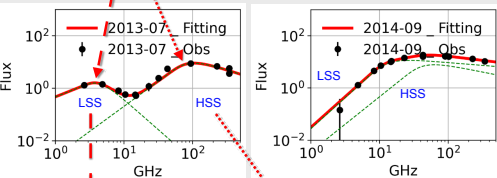


Fig 3. Two examples of double SSA features of 3C 454.3 before (Left) and after (Right) 2014 Jun  $\gamma$ -ray flare.

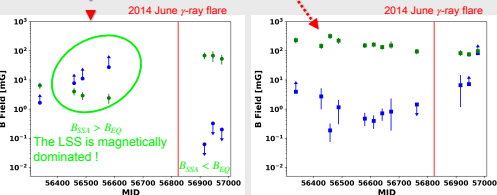


Fig 4. B-field estimation for both LSS (Left) and HSS (Right). Arrows are upper and lower limits. Blue and green dots are B-field strength of SSA region ( $B_{SSA}$ ) and equipartition condition ( $B_{EQ}$ ), respectively.

## 5. B-Field Strength Estimation

By using the estimated turnover frequency ( $\nu_m$ ) and peak flux density ( $S_m$ ), and interpolated size ( $d_m$ ) of SSA emitting region from jet geometry, we estimated B-field strength for both SSA region and equipartition condition (Fig4). Higher  $B_{SSA}$  than  $B_{EQ}$  of the LSS indicates the LSS emitting region is magnetically dominated. The formulas of  $B_{SSA}$  and  $B_{EQ}$  were referred from Marscher (1983) and Kataoka & Stawarz (2005), respectively. In the estimation, we inferred the dimensionless factor  $b(\alpha)$  from Table 1, in Marscher (1983), and we assumed  $\eta$  as 100 which is the ratio of energy density between proton and electron.

$$B_{SSA} = 10^{-5} b(\alpha) \left[ \frac{S_m}{1 \text{ Jy}} \right]^{-2} \left[ \frac{d_m}{1 \text{ mas}} \right]^4 \left[ \frac{\nu_m}{1 \text{ GHz}} \right]^{-3} \frac{1+z}{\delta} \text{ [G]}$$

$$B_{EQ} = 0.123 \times \eta^{\frac{1}{2}} \times (1+z)^{\frac{1}{2}} \times \left[ \frac{D_L}{100 \text{ Mpc}} \right]^{-\frac{1}{2}} \left[ \frac{\nu_m}{5 \text{ GHz}} \right]^{\frac{1}{2}}$$

$$\times \left[ \frac{S_m}{100 \text{ mJy}} \right]^{\frac{1}{2}} \left[ \frac{d_m}{0.3''} \right]^{-\frac{1}{2}} \times \delta^{-\frac{1}{2}} \text{ [mG]}$$

Marscher (1983) Kataoka & Stawarz (2005)

$\delta$ : Doppler factor  
 $z$ : redshift  
 $D_L$ : Luminosity Distance

## 6. Correlation of the SSA Spectra with Core

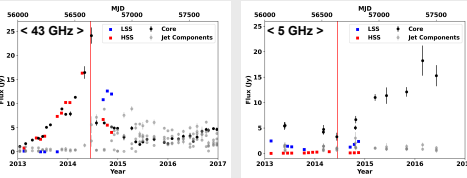


Fig 5. Comparisons between SSA-inferred flux variation and VLBI flux measurements at both 43GHz (Left) and 5GHz (Right). Black and grey dots indicate core and jet components, respectively.

- HSS-inferred flux variation  $\sim$  43 GHz core flux variation
- LSS-inferred flux variation  $\sim$  5 GHz core flux variation ?
- The HSS emitting region is the radio core at 43GHz.
- Then, where is the LSS emitting region?

## 7. Spectrum of the Component C

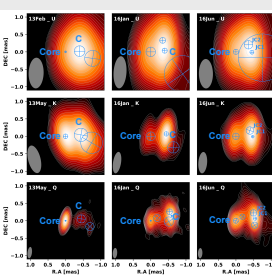


Fig 6. Multi-frequency VLBA maps at three epochs (Left) and spectrum of the component C (Right). Colors and contours in Left panel indicate Stokes I intensity.

- Component C from the multi-frequency VLBA observations.
- Optically thin spectrum before 2014 June  $\gamma$ -ray flare.
- Optically thick  $\sim$  flat spectrum after 2014 June  $\gamma$ -ray flare.
- The LSS emitting region is the component C. (Compare with Fig 3.)
- Stationarity & B-dominated region of the component C
- Recollimation shock ?

## 10. Conclusions

The multi-wavelength observations allow us to find spectral feature of the blazar 3C 454.3, and we found two individual SSA features, the LSS and the HSS. Moreover, by using the multi-frequency VLBA observations, we found the quasi-stationary (C) component  $\sim 6 \times 10^5 r_g$  from its central black hole and found this feature is the LSS emitting region. From the B-field strength estimation, we found the LSS emitting region is magnetically dominated.

Analysis of jet ridgeline and polarization maps show jet collimation within the component C. And its DoP is higher than the radio core. Interestingly, the most of the BU 43 GHz observations show parallel EVPA with jet axis at the component C as far as it is observed. These results may indicate the component C of 3C 454.3 is recollimation shock.

## 8. Jet Size along the Ridgeline

- Stack : Stokes I maps from 2013 Jan  $\sim$  2016 Dec at 43 GHz
- Common circular restoring beam of  $0.2 \text{ mas} \times 0.2 \text{ mas}$
- Jet ridgeline by selecting highest brightness pixels in radially
- Core position offset from Kutkin et al. 2014
- Uncertainties were estimated by following Pushkarev et al. 2017

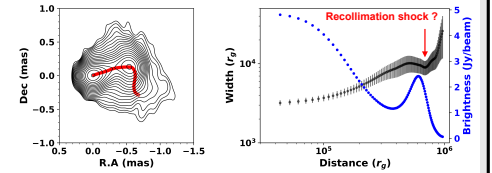


Fig 7. Left : Stacked BU Stokes I maps. Red circles indicate jet ridgeline. Right : Estimated jet width and brightness along the ridgeline.

- Parabolic expansion up to  $\sim 5 \times 10^5 r_g$
- Secondary brightness peak  $\sim 6 \times 10^5 r_g$
- Maximum collimating point  $\sim 7 \times 10^5 r_g$
- Conical / hyperbolic expansion beyond collimating zone
- Recollimation shock ?

## 9. Stacked Polarization Maps

Stack : same with section 8.

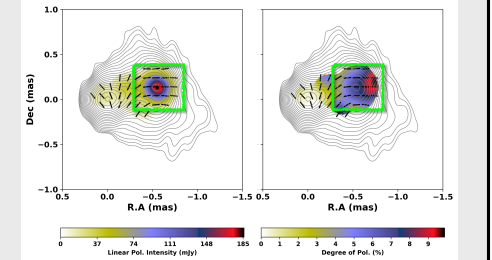


Fig 8. Stacked polarization maps of 3C 454.3. Colors indicate linear polarization intensity (Left) and degree of linear polarization (Right).

- Higher linear polarization intensity at the component C than 43 GHz core
- Higher degree of linear polarization (DoP) at the component C than 43 GHz core
- Parallel electric vector position angle (EVPA) with jet axis
- Recollimation shock !

## References

Fuhrmann et al. 2016, A&A, 596, A45  
Liodakis et al. 2020, ApJ, 902, 61

Jorstad et al. 2017, ApJ, 846, 98  
Lister et al. 2018, ApJS, 234, 12

Kataoka & Stawarz 2005, ApJ, 622, 797  
Marscher 1983, ApJ, 264, 296

Kutkin et al. 2014, MNRAS, 437, 3396  
Pushkarev et al. 2017, MNRAS, 468, 4992